Bulletin of the Seismological Society of America, Vol. 94, No. 3, pp. 1016–1035, June 2004

Degree of Polarization Filter for Frequency-Dependent Signal Enhancement Through Noise Suppression

by M. Schimmel and J. Gallart

Abstract We construct and examine a new frequency-dependent polarization filter to attenuate less polarized signals and noise in single and multichannel seismic data. The filter uses a degree of polarization measure which is defined as a measure of the variations of an arbitrary instantaneous polarization through the course of the signal. Small variations indicate a high degree of polarization. The frequency-dependent degree of polarization is based on the eigen analysis of the data covariance matrices and is used to weight the decomposed time series in the time-frequency domain. This approach permits the frequency-dependent detection of polarized signals and their enhancement through less polarized signal and noise suppression. Further, interfering signals with different frequency contents can be separated. With densely spaced data the degree of polarization can be averaged locally to include the wave-field directivity. This procedure is important since, through the averaging, isolated polarized noise can be removed, but isolated unpolarized signals are not suppressed. In contrast to waveform stacks or stacks of data covariance matrices our approach does not punish signals with spatially changing characteristics, such as happens in the transition from precritical to postcritical reflections. Our data adaptive filter is analyzed with theoretical test data before it is applied to a complex wide-angle record section from the West Pyrenees.

Introduction and Motivation

The determination of seismic structure in the Earth is essentially based on the combination of the study of seismic wave propagation, the measurement of seismic ground motion, and the identification and interpretation of seismic signals in seismograms. The study of seismic signal detection and interpretation is therefore important and has provided numerous tools which are constantly improved to come up with new data volumes and new measurement configurations and to increase the routine extraction of information in the seismograms.

Not all types of processing methods are adequate for the different data sets because of the variability of the measurement geometry and the variability of signals and noise. The methods to apply depend on the geometry and the domain (time, slowness, frequency, waveform, *et al.*) where signal and noise can mostly be distinguished. The polarization filters form part of these signal detection and identification tools. They separate signals from noise by their polarization which is usually measured on three-component (3-c) data.

In this article we report our attempt to construct a frequency-dependent polarization filter that is based on a new definition of the degree of polarization. The degree of polarization is aimed to measure how well a signal is polarized independently of its type and direction. Such measure can be applied to attenuate the less polarized signals and noise components.

Polarization analyses have been used for a long time (Montalbetti and Kanasewich, 1970; Kanasewich, 1981; Samson, 1983; Vidale, 1986; Christoffersson *et al.*, 1988; Perelberg and Hornbostel, 1994; Lilly and Park, 1995; Reading *et al.*, 2001; De Franco and Musacchio, 2001). Most of these studies are based on directional pass filters. Signals with predefined polarization characteristics such as azimuth, take-off angle, linearity, or ellipticity are passed by these filters while the remaining signals are attenuated following their deviation from the predefined attributes. These attributes are usually derived in the frequency domain (e.g., Samson, 1983; Park *et al.*, 1987) or in the time domain (e.g., Kanasewich, 1981; Vidale, 1986; Bataille and Chui, 1991). Some approaches are time-frequency hybrids (e.g., Jurkevics, 1988), and other methods use the analytic signals (e.g., Vidale, 1986; Bataille and Chui, 1991; Morozov and Smithson, 1996; Schimmel and Gallart, 2003).

Most techniques are based on an eigen analysis of the data covariance matrix constructed in the time or the frequency domain. The matrices are determined for sliding data windows to decompose the data into their principal energy components (e.g., Samson, 1983; Jackson *et al.* 1991) given

by eigenvalue-eigenvector pairs. This decomposition is used to derive the polarization as function of time or time and frequency, respectively. The success of these methods depends on the selection of the analysis window, which is subject to dominant periods, signal-to-noise energy ratio, signal durations, and signal separations. The polarization studies are sensible to noise, and the averaging of the covariance matrixes or waveforms (e.g., Jurkevics, 1988; Bataille and Chui, 1991) or of the degree of polarization (Schimmel and Gallart, 2003) permit improved signal resolution and noise attenuation.

The eigenvalues of the spectral data matrix can be used to design a frequency-dependent degree of polarization (Samson and Olson, 1980). Samson and Olson (1980) create this measure to determine whether the spectral matrix represents a pure state, that is, whether it can be decomposed by one eigenvalue-eigenvector pair. The eigenvectors are complex and therefore describe linear and elliptical motion. This approach is energy biased and polarized signals with separate polarizations (e.g., *SH* and *SV* waves) that are decomposed into two principal directions are attenuated when considering how much the spectral matrix is represented by one eigenvalue-eigenvector pair. The degree of polarization determination has been expanded by Du *et al.* (2000). They incorporate the multitaper approach (Park *et al.*, 1987) to diminish spectral leakage and perform a noise decontamination by using a noise estimate from a presignal window. The modifications make the degree of polarization more sensitive, which can improve the filter performance.

Schimmel and Gallart (2003) present an alternative definition for the degree of polarization that is based on the variability of arbitrary polarization directions through the course of the signals. Their measure uses a variational approach for analytic signals (Morozov and Smithson, 1996) to obtain instantaneous polarization attributes without the need of an eigen analysis. It handles linear and elliptical motion. The measure is frequency independent and designed to detect time-separated polarized signals. Their filter does not permit the detection of polarized signals that are hidden in noise with different frequency contents. Only a frequency-dependent strategy can deal with such data. Here, we report a polarization filter that uses a frequency-dependent degree of polarization based on the principles presented in Schimmel and Gallart (2003). The filter concept, however, is different. For instance, we use no analytic signals and use an eigen analysis to obtain instantaneous frequency-dependent polarization attributes. In the following we outline and discuss the method, we examine examples with theoretical test data, and apply the filter to a complex wide-angle reflection/refraction profile from the West Pyrenees in Spain.

Frequency-Dependent Degree of Polarization Filter

In this section we introduce the frequency-dependent degree of polarization measure which can be used for seismic signal enhancement through frequency-dependent noise suppression. The signals are determined by small variations in their arbitrary polarization on a sample-by-sample basis. The polarization is measured as a function of frequency and time based on a principal component analysis for sliding data windows. The degree of polarization is determined in analogy to the strategy by Schimmel and Gallart (2003). We first outline their approach and then explain the frequency-dependent method.

Time-Domain Degree of Polarization Filter

The instantaneous polarization attributes, such as semimajor and semiminor axes, are determined according to Morozov and Smithson (1996). Their method is based on the analytic signal vector formed by the complex traces of the triaxial data system. A variational approach is used to determine the instantaneous attributes without need of an eigen analysis of the covariance data matrices.

The filter by Schimmel and Gallart (2003) uses the semimajor vector $\vec{a}(t)$ and the planarity vector $\vec{p}(t)$ of the ground-motion ellipse. The planarity vector is defined by the vector cross product of the semimajor and semiminor vector. Vector $\vec{p}(t)$ is perpendicular to the surface of the motion ellipse and does not change the direction for planar (prograde or retrograde) motion.

The degree of polarization $c(t)$ is based on the variation of the unit planarity or unit semimajor vector with respect to their mean direction determined within a sliding window of length T. The variation is measured in terms of vector projections as shown in equation (1).

$$c(t) = \left(\frac{1}{1 + T} \sum_{\tau = t - T/2}^{t + T/2} \left| \frac{\vec{m}(t)}{|\vec{m}(t)|} \cdot \frac{\vec{x}(\tau)}{|\vec{x}(\tau)|} \right|^{v_1} \right)^{v_2} \tag{1}$$

with mean vector $\vec{m}$

$$\vec{m}(t) = \frac{1}{1 + T} \sum_{\tau = t - T/2}^{t + T/2} \frac{\vec{x}(\tau)}{|\vec{x}(\tau)|} \tag{2}$$

and polarization attribute $\vec{x}(t)$

$$\vec{x}(t) = \begin{cases} \vec{a}(t) : l(t) > 0.7 \\ \vec{p}(t) : \text{else} \end{cases} \tag{3}$$

In equation (1) we add the projections of the instantaneous semimajor or planarity unit vectors onto their unit mean vector. The exponents v_1 and v_2 are positive numbers to control the sensitivity of noise attenuation. The exponents act on the individual vector projections and on their sum, respectively. They increase the differences between polarized and less polarized signals. Usually, it is not important how these differences are increased and we simply use $v_1 = v_2 = v$. $c(t)$ ranges between 0 and 1. $c(t) = 1$ indicates that the signal is perfectly polarized at time t. Signals that are not well polarized cause small $c(t)$ values. $l(t)$ is the rectilinearity defined by the ratio of the semiminor $|\vec{b}(t)|$ to the semimajor

$|\vec{a}(t)|$. It is expressed as $l(t) = 1 - \frac{|\vec{b}(t)|}{|\vec{a}(t)|} = 1 - \frac{|\vec{p}(t)|}{|\vec{a}(t)|^2}$. $l(t)$ ranges between 0 and 1, with 1 assigning perfect linear motion. From equation (3) we see that the semimajor $\vec{a}(t)$ is only used in $c(t)$ for linear or almost linear motion. This, since vector $\vec{a}(t)$ becomes ambiguous for almost circular motion due to noise contamination which may transform semiminor to semimajor axes. Similarly, the planarity vector is only defined for elliptical motion. For linear motion the semiminor is small and strongly affected by noise. Consequently, the direction of $\vec{p}(t)$ is not stable. The attribute choice in equation (3) bypasses these problems. In practice, we use a moving average of $\hat{l}(t)$ in equation (3). The filtered traces are obtained by the multiplication of the degree of polarization $c(t)$ with the unfiltered data.

The filter procedure is illustrated in Figure 1. The top panel contains theoretical test data with a polarized signal which is marked by the gray background. We use the sample index rather than the time values to simplify the comparison with small data windows that we use in the following. The small- and large-amplitude noise is random noise that has been built from the signal-amplitude spectrum. Below, the instantaneous semimajor and planarity vectors are shown for three seven-sample data windows using an orthographic azimuthal projection. The semimajor vectors are depicted in the first line, and the planarity vectors are indicated in the second line. The center position of the windows are indicated by the dotted lines. The black dot in the projection center of each sphere is the mean vector in the considered data window. It can be observed from these spheres that the instantaneous vectors vary only little from their mean direction for the polarized signal. Consequently, their projections onto the mean vector are large and add to large degree of polarization values throughout the course of the signal following equations (1)–(3). The three lower-most traces in Figure 1 are the filter output obtained by the product of the test data with the degree of polarization $c(t)$ (equation 1).

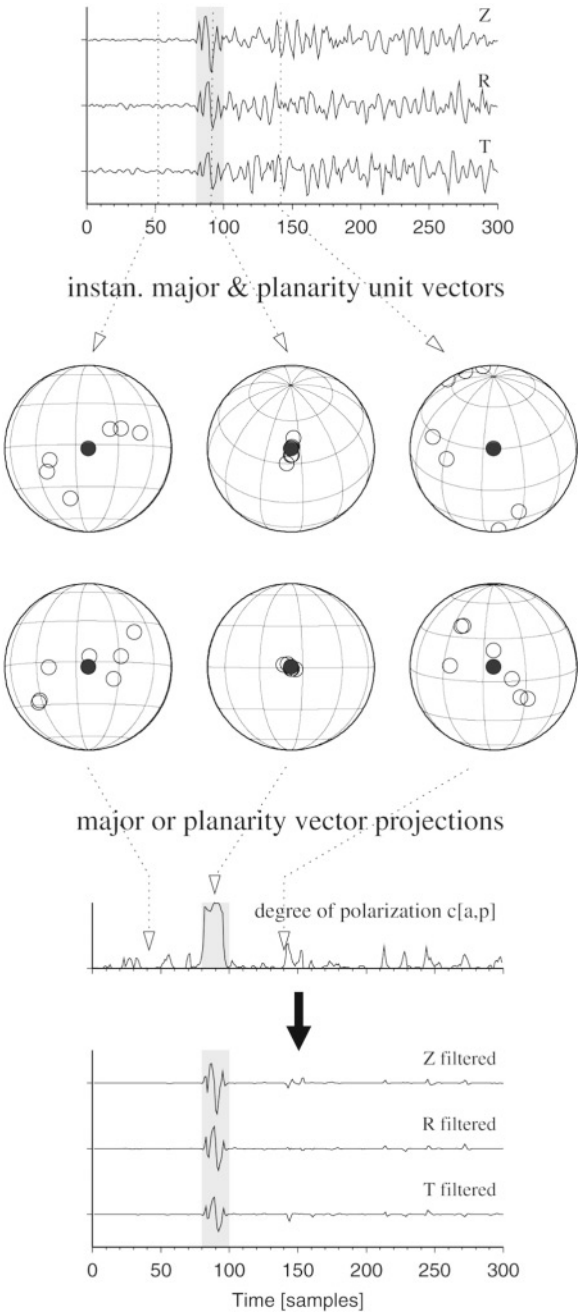

Figure 1. The figure outlines the time-domain degree of polarization filter. The 3-c test data contain a polarized signal (gray background) and random noise built from the signal-amplitude spectrum. The hemispheres show the perspective projections of the semimajor (first line) and planarity unit vectors (second line) for three seven-sample windows. The dotted line, open circles, and black dots mark the window centers, the instantaneous vectors, and their mean vector. The degree of polarization is obtained from the vector projections within a sliding seven-sample data window. The filtered data result from a multiplication of the records with the degree of polarization.

Frequency-Dependent Degree of Polarization Filter

The frequency-dependent approach uses a different philosophy than the method just outlined. The analytic signal theory is not used to obtain an instantaneous polarization measure. Here, we perform the eigen analysis of the cross spectra of sliding data windows to obtain the eigen values and vectors as function of frequency and time. This way we obtain a frequency-dependent degree of polarization measure which is used to attenuate the less polarized frequency components of the data. Then, the inverse transform is taken to obtain the filtered traces. The sliding time window enables the time-frequency analysis of the time series.

Eigen Approach for the Triaxial Data Matrix and Polarization State. The cross spectrum $\mathbf{S}(\omega) = \vec{z}(\omega)\vec{z}(\omega)^{\tau}$ is a complex 3×3 matrix for each frequency ω. $^{\tau}$ stands for conjugate complex and $\vec{z}(\omega)$ is the Fourier transform of the

real data vector $\vec{x}(t)^T = [x_1(t), x_2(t), x_3(t)]$, which consists of the windowed 3-c seismic registration. The cross spectrum $\mathbf{S}(\omega)$ can be decomposed into eigenvalues λ and eigenvectors $\vec{v}$ as shown in equation (4).

$$\mathbf{S}(\omega) = \sum_{l=1}^{3} \lambda(\omega)_l \vec{v}(\omega)_l \vec{v}(\omega)_l^{\tau} \tag{4}$$

Matrix **S** is conjugate-symmetric (Hermitian) and the eigenvalues are therefore non negative. The eigen vectors can be complex and form an orthonormal basis for the signal vectors. In the following, we suppress the ω dependence as long as it is not explicitely important for the understanding. If $\lambda_1 \gg \lambda_2, \lambda_3$ then the polarization is well determined by the eigenvector $\vec{v}_1$. Phase lags between the complex components of the vector represent the elliptical particle motion. The case that λ_1 is the only non-zero eigenvalue is called pure state (Samson and Olson, 1980), because the wave is purely polarized. Samson and Olson (1980) define a degree of polarization measure P^2 (equation 5) to determine whether the spectral matrix represents a pure state.

$$P^2 = \sum_{j,k=1}^{3} (\lambda_j - \lambda_k)^2 / \left[4 \left(\sum_{j=1}^{3} \lambda_j \right)^2 \right]. \tag{5}$$

P ranges between 0 and 1, where 1 assigns the pure state of the matrix **S**.

With $\lambda_1 \approx \lambda_2$ we obtain $P \approx 0$. For $\lambda_1 \approx \lambda_2 \gg \lambda_3$ there is a strong possibility that there are signals with two separate polarizations (Park *et al.*, 1987). Their superposition is decomposed into two orthogonal directions by two eigenvectors and eigenvalues. The signals must not have orthogonal polarization such as *SV* and *SH* motion, and a separation into the two signals is only possible with additional informations.

If **S** represents a pure state then the semimajor and semiminor vector of the motion ellipse can be determined from the first eigenvector $\vec{v}_1$. The vector is rotated in the complex domain by a phase Φ such that $\vec{v}_1 \exp(i\Phi) = \vec{a} + i\vec{b}$, where $\vec{a}$ and $\vec{b}$ are mutually orthogonal vectors in a real space ($\vec{a}^T\vec{b} = 0$). The rotated vector $\vec{v}_1$ remains an eigenvector of matrix **S** despite the rotation. Choosing $|\vec{a}| > |\vec{b}|$ then $\vec{a}$ and $\vec{b}$ are the directions of the semimajor and semiminor axes of the polarization ellipse for sinusoidal waves. Samson and Olson (1980) call these vectors state vectors and provide two ways to determine their directions. Another approach can almost directly be adopted from Morozov and Smithson (1996). In the following we explain how these vectors $\vec{a}$ and $\vec{b}$ are used to build the frequency-dependent degree of polarization filter.

Measuring the Degree of Polarization. The cross spectrum and the corresponding polarization attributes are determined for sliding data windows. We use Gaussian-shaped windows $g(t)$ and keep the option to stabilize the cross spectra over $(2\delta + 1)$ frequencies.

The cross spectrum estimate then becomes

$$\hat{\mathbf{S}}(t, \omega) = \frac{1}{2\delta + 1} \sum_{k=\omega-\delta}^{\omega+\delta} \vec{z}(t, k) \vec{z}(t, k)^{\tau} \tag{6}$$

where

$$\vec{z}(t, k) = \sum_{\tau=t-T/2}^{\tau=t+T/2} g(t - \tau) \vec{x}(\tau) \exp(-ik\tau) \tag{7}$$

and ω, δ, k, and t, τ are the frequency and time indices, respectively. In equations (6) and (7), t is the center time of the Gaussian-shaped window and T is the length of the window. As a consequence of the time-frequency description, the degree of polarization from equation (1) becomes a time-frequency matrix $c(t, \omega)$, where t is the center time of the sliding data windows.

$c(t, \omega)$ is determined by using the vectors $\vec{a}$ and $\vec{b}$ obtained from the eigenvector $\vec{v}_1$. Only if $\lambda_1 \gg \lambda_2, \lambda_3$ ($P \approx 1$) then the vectors $\vec{a}$ and $\vec{b}$ correspond to the true polarization ellipse. In general, it is assumed that this case describes the data at most instances. If $\lambda_1 \approx \lambda_2$ then the signal at frequency ω is decomposed into more than one direction. P is very small and the spectral matrix is not in a pure state. Nevertheless, we consider the first principal direction $\vec{v}_1$, which, in general, does not coincide with a polarization vector of one of the superimposed signals. Therefore, vectors $\vec{a}$ and $\vec{b}$ do not represent anymore the true ground-motion ellipse. Still, the stability of these vector directions can be used as measure of the degree of polarization. The little variation of the unit vectors can indicate the presence of polarized signals that we do not want to attenuate. These signals interfere in time and frequency and can only be separated by their principal components if the polarization is orthogonal such as for the superposition of *SH* and *SV* waves.

The local spectrum $\vec{z}(t, k)$ is obtained using a Gaussian envelope. We keep the option to make its width frequency dependent. The use of a constant window width implies that the time resolution is the same for all spectral components. Conversely, with the frequency-dependent window one maintains a constant number of periods in the window and has therefore an invariant frequency resolution. Other windows can replace $g(t)$, depending of the special needs of the analysis.

Frequency-Dependent Noise Reduction. The degree of polarization measure $c(t, \omega)$ is used to attenuate the less polarized frequency components of the Fourier transform of the windowed data. This is performed by a simple multiplication of $c(t, \omega)$ with the data in the frequency domain. The filtered traces $y(t)$ are obtained after the inverse transformation to the time domain and can be expressed as:

$$y(t) = \frac{1}{2\pi T} \int_{-\infty}^{\infty} c(t, \omega) z(t, \omega) \exp(i\omega t) d\omega. \tag{8}$$

$c(t, \omega)$ is attained from the triaxial input data and, therefore, equation (8) describes a data-adaptive filter. If $c(t, \omega)$ is rough, then it is recommended to stabilize the inverse transform by smoothing the degree of polarization matrix. A simple averaging procedure such as $\hat{c}(t, \omega) = (1 + 2\delta)^{-1} (1 + 2\tau)^{-1} \sum_{\omega-\delta}^{\omega+\delta} \sum_{t-\tau}^{t+\tau} c(t, \omega)$ can already provide good results. As shown later, we often run first a median filter to remove possible outliers before they get blurred by the mean filter (Schimmel and Gallart, 2003). We do not compute the degree of polarization function at all frequency components. Using a coarser sampling and an interpolation scheme to fill the gaps is generally possible. However, $\hat{\mathbf{S}}$ from equation (6) should be determined by using the smallest frequency (fundamental frequency) increment.

Including the Wave-Field Directivity. For densely spaced data the efficiency of the filter can be increased by including the directivity of the wave fields. This can be done by a scheme that considers the coherence of the wave field over space. In Schimmel and Gallart (2003), we successfully showed that one can average the degree of polarization rather than the waveforms or covariance matrices. This procedure does not down-weight polarized signals with spatially changing waveforms, such as occurs at the transition between pre- and postcritical reflections or due to focusing/defocusing by heterogeneous structure. Further, isolated polarized signals can be suppressed, whereas the averaging can prevent the attenuation of isolated unpolarized signals.

Schimmel and Gallart (2003) use for linear record sections a local slant-stack strategy within a sliding time-distance window across the degree of polarization section. Their local averaging scheme has been extended to include the frequency and can be expressed as follows:

$$\hat{c}(\omega, t, r) = \max\{\tilde{c}(\omega, t, r, p_j)\}_{j=1, J} \tag{9}$$

with

$$\tilde{c}(\omega, t, r_i, p_j) = N \sum_{k=-K}^{K} \sum_{m=i-M}^{i+M} \sum_{l=-L}^{L} c(\omega + k\delta\omega, t + (r_m - r_i)p_j + l\delta t, r_m) \tag{10}$$

and

$$N = (1 + 2M)^{-1}(1 + 2K)^{-1}(1 + 2L)^{-1}, r = r_i. \tag{11}$$

$\hat{c}(\omega, t, r)$ is the averaged degree of polarization that is used in the filter. p_j values are discrete slowness values within the range of J realistic slowness values for the signals. δt and $\delta\omega$ are the time and frequency intervals and r is the station distance to a reference point, such as the source location. $1 + 2M$ defines the number of traces used in the averaging, whereas K and L permit the inclusion of neighboring frequency and time samples. In practice, we keep K and L small, that is, equal 1 and determine the median instead of the mean to remove outlying isolated features in the polarization matrix rather than blurring these signals by applying the mean.

The averaging can be an important filter stabilizator because the polarization is not a robust measure to noise contamination. Noise can be polarized itself or can unpolarize polarized signals. The spatial averaging removes the isolated polarized noise or inhibits the attenuation of the isolated unpolarized signals. Latter means that if an unpolarized signal is aligned between polarized signals, then the averaging can raise the low degree of polarization for the unpolarized signals. Consequently the signal is less attenuated.

Synthetic Examples

First Example: White-Noise Contamination

The functioning of the filter is illustrated with synthetic case studies. First, we consider three polarized signals contaminated with random white noise. The noise-free and noise-contaminated time series are the top two traces in Figures 2a–c. The signals 1, 2, and 3 (labeled in Fig. 2a) have different elliptical polarization and have been obtained by filtering a random time series. Their center frequencies are 4.5, 8.5, and 11 Hz with sample interval of 16 ms. The traces are shown with their sample index to enable a better comparison with the small data windows used in the filter. The amplitude spectra of the noise-free signals and the white background (BG) noise are shown in Figure 2d. The noise-contaminated traces form the input data of our filter.

The third traces in Figure 2a–c show the filter outputs obtained using Gaussian-shaped data windows [$g(t)$ in equation 7] with twice the standard deviation (2σ) equal 19 samples to determine the instantaneous polarization ellipse (planarity and semimajor vector) through their cross spectra (equation 6). The degree of polarization is obtained from the instantaneous attributes with sliding windows of nine samples and power $v = 32$ (equation 1). For brevity we name these windows 2σ window and DOP window, respectively. The degree of polarization has been computed at 50 frequencies between 0.3 and 17 Hz, using every second frequency in the spectral domain. The frequency values are marked by the inverted triangles at the top of Figure 2d. Further, the measure has been smoothed with a three-sample window in time and frequency. This is almost a default smoothing, which one can apply before the backtransformation to the time domain to avoid artifacts that may arise for rough functions. Filter outputs (Z components) obtained with alternative values for the 2σ and DOP windows are shown in Figure 2e. These traces permit access to the waveform changes for alternative settings. Altogether, the filter outputs show a clear noise attenuation. A similar noise suppression can not be achieved with a bandpass filter. The signals have different frequency contents that together cover a broad frequency range (Fig. 2d). This means that the bandpass requires a broad band to keep the signals and, consequently, the noise in a broad frequency range.

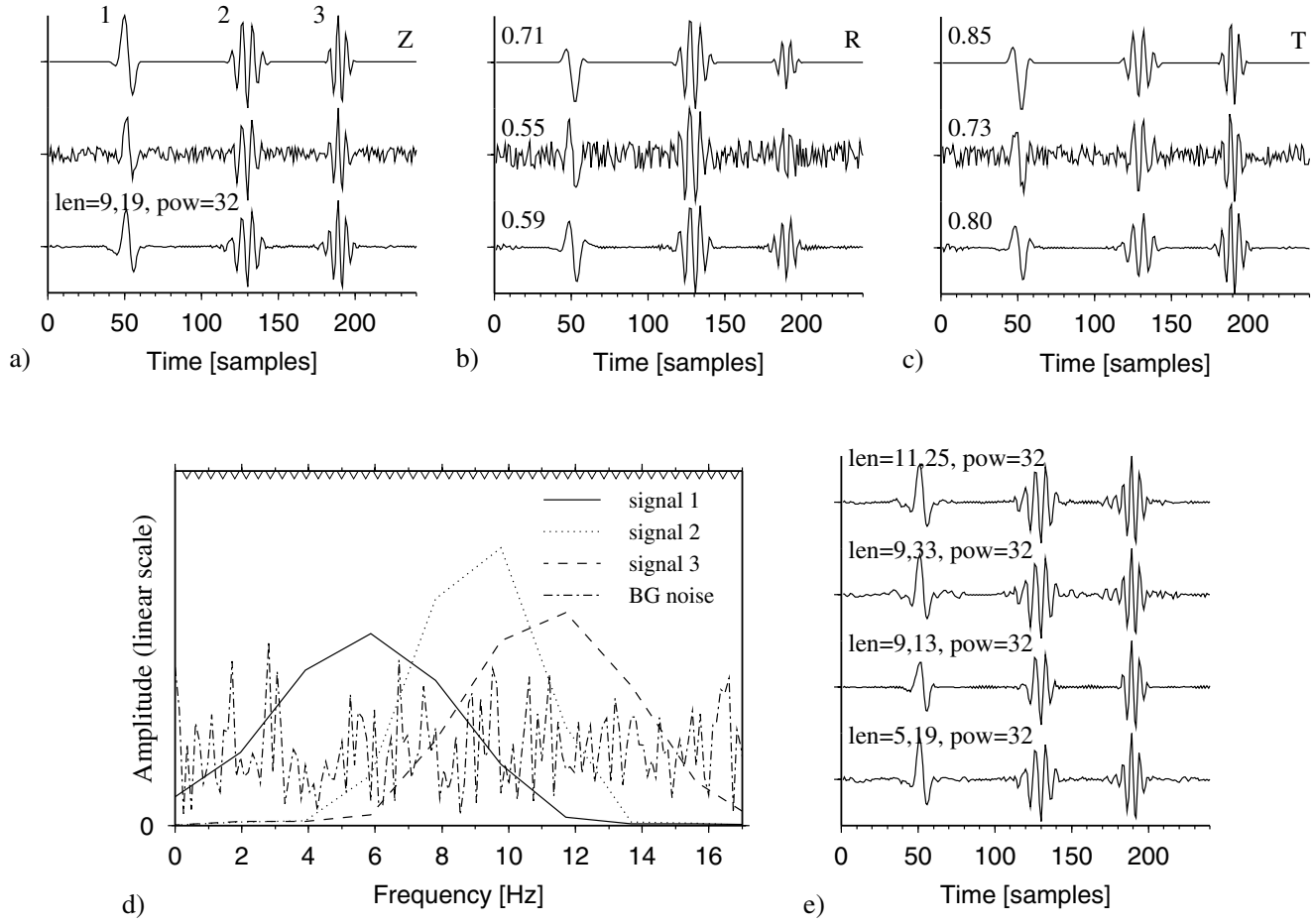

Figure 2. (a) From top to bottom: noise-free vertical component (*Z*) record, same record with white-noise contamination, and filter result. The *len* values are the DOP and 2σ window length in sample units. (b) and (c) are the same as (a), except for the radial (*R*) and transverse (*T*) components. The numbers at the upper left are the relative amplitudes with respect to the corresponding Z trace. (d) The amplitude spectra are from the three signals and the background (BG) noise. (e) The *Z*-component filter outputs for different parameters.

The degree of polarization of the noisy traces in Figure 2a–c is contoured in Figure 3a. The contouring starts at 0.2 (gray lines) and 0.8 (black lines), which correspond to 20% and 80% of the theoretical maximum amplitude. The contour intervals are 0.1 and 0.05 for the gray and black lines, respectively. From this figure several maxima with different amplitudes are identified. Most of these maxima are isolated features in time and frequency and can be attributed to randomly polarized noise components. The three signals (Fig. 3) are identified by their large polarization at the expected time (gray background) and their dominant frequencies. The high amplitudes at the first samples are artifacts due to the windows that partly cover the data when centered at the first samples. These effects can be avoided by damping or increasing the time series, such as done at the end of the time series. The first trace in Figure 3e shows the filter output obtained using the degree of polarization matrix from Figure 3a. It can be seen from the filter output that the artifacts or isolated polarized noise components do not strongly affect the time series.

The impact of the isolated features in the degree of polarization matrix onto the filtered time series depend on their amplitudes and the phase and amplitude spectra of the signals. In this and the other examples in this article, a stabilization of the degree of polarization matrix is not needed. Nevertheless, if required, then the isolated outlying signals are generally easy to remove as illustrated with Figure 3b and c. Figure 3b shows the degree of polarization after smoothing the values using their median in a sliding data window of three time samples $\times$ three frequency samples. This procedure can be repeated several times until stationarity is archived, that is, when further iterations will not significantly alter the matrix. In Figure 3c and d we show the degree of polarization matrix after applying the median filter 3 and 50 times, respectively. After the last median filter iteration a mean filter with the same three-sample window is

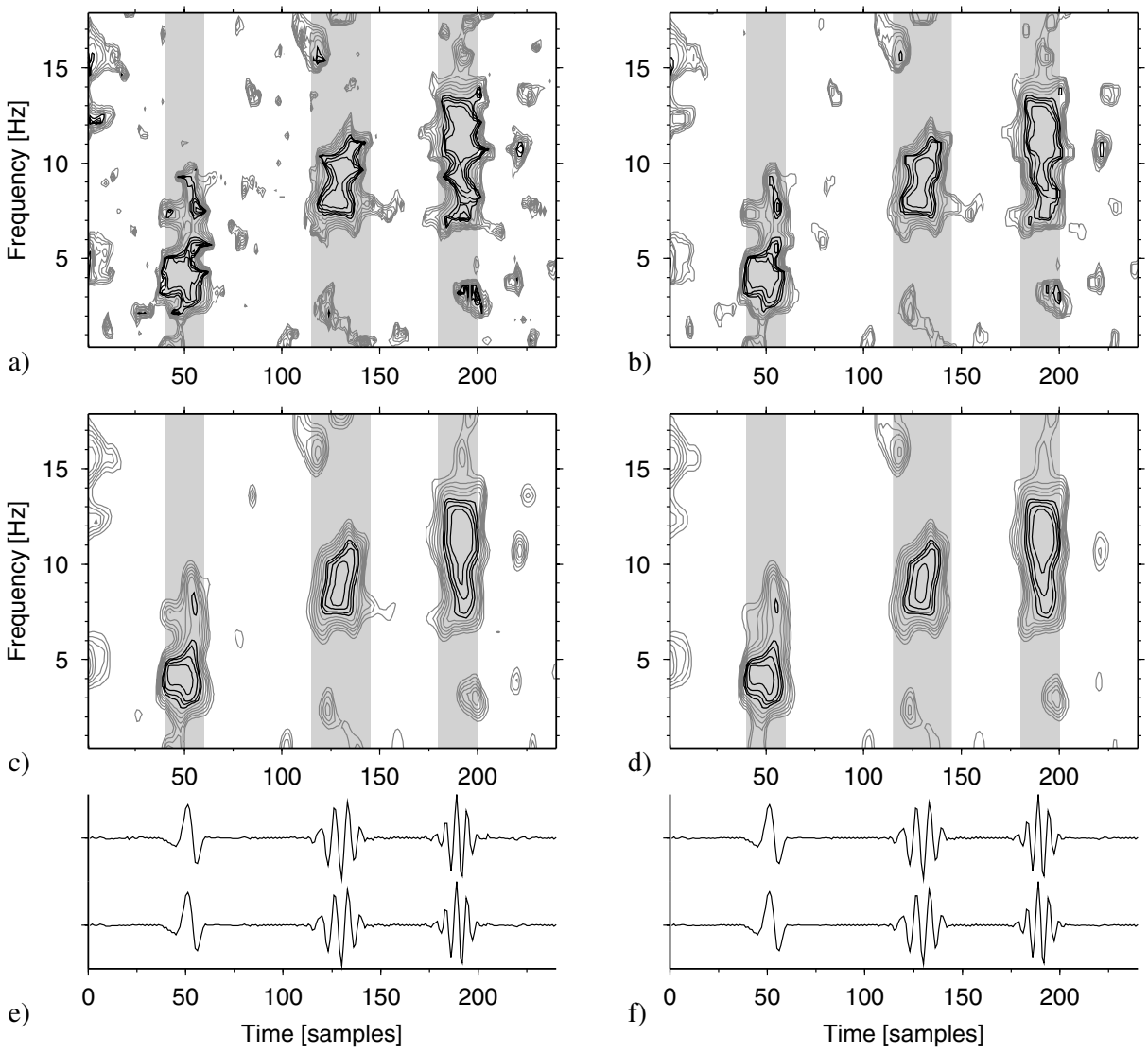

Figure 3. The degree of polarization of the noisy data (Fig. 2) is contoured as a function of time and frequency. The contouring starts at 0.2 (gray lines) and 0.8 (black lines) with intervals of 0.1 and 0.05, respectively. The gray background marks the time of the three signals. In (a), the degree of polarization is not smoothed, and in (b), the matrix is smoothed by a 3×3 median filter. (c and d) The results after applying 3 and 50 times the same median filter and afterward a 3×3 mean filter. (e) and (f) contain the filter output obtained with the matrices from panels (a) and (b) and (c) and (d), respectively.

applied for additional smoothing. The time series in Figure 3e and f are the filter outputs using the degree of polarization matrix from Figure 3a–d. Figure 3 shows that the median removes the isolated outliers and preserves the signal shapes, but one final mean iteration can further smooth the amplitudes. Using only the mean would blur the isolated spikes. The degree of polarization matrix can be processed in many different ways. For instance, at this stage interfering polarized signals with different frequency contents can be isolated for individual reconstructions by attenuating the undesired elements in the matrix.

In Figure 4a and b we illustrate the mean dependence of the filter output on the power, and the DOP and 2σ windows in terms of waveform similarity and signal-to-noise (S/N) energy ratio. For this analysis we use time series with three signals and white noise such as shown in Figure 2a–c. To remove the dependence to a special waveform or noise realization we compute 22 different data sets with random signal waveforms and noise realizations. These data sets have been filtered using the filter settings from Figure 4a and b. The filtered signal waveforms have been correlated with the noise-free signal waveforms to measure their waveform similarity. The values have been averaged for each filter setting and are illustrated in Figure 4a. A high correlation means a good waveform recovery or, alternatively, a low waveform distortion.

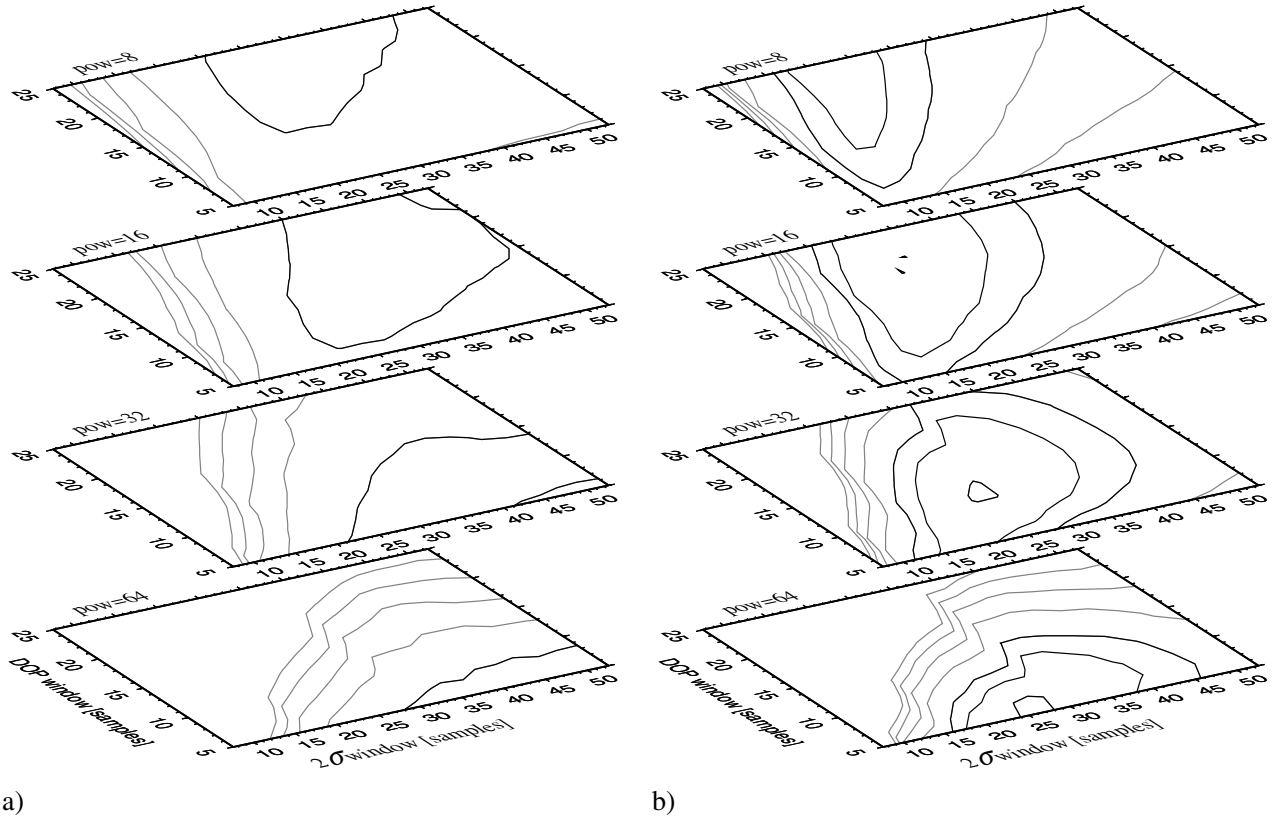

Figure 4. (a) The PCC waveform similarity between filtered and noise-free signals is contoured as function of power, DOP and 2σ window length. Contouring starts at 0.5 (gray lines) and 0.7 (black lines). The maximum correlation determined with a conventional cross-correlation is 0.944. (b) The natural logarithm of the signal-to-noise energy ratio (see text) is contoured from 1.6 with interval 0.1 (gray lines) and from 2 with interval 0.05 (black lines). The values in (a) and (b) are the mean values obtained with 22 different random signal-and-noise realizations.

In Figure 4a, we show the zero lag phase cross-correlation (PCC) values (Schimmel, 1999) since PCC is more sensible to waveform coherence than the conventional energy normalized cross-correlation. PCC is based on complex trace analysis. Roughly, PCC measures the similarity by the number of coherent samples rather than by using the sum of energy cross products and is therefore less energy biased. The conventional energy cross-correlations have also been computed and show a similar trend to PCC with overall higher values (maximum mean correlations are 0.944) and a slightly less pronounced maximum.

Further, we use the filtered traces to determine the energy ratio S/N $= (S_i + S_o)n_n/((N_i + N_n)n_s)$, where S_i, N_i and S_o, N_o are the energy values for data stretches with signals (S) and with pure noise (N) on the vertical component filter input (i) and output (o). n_n and n_s are the number of the corresponding noise and signal samples. S_i and N_i stabilize the ratio for low-energy filter outputs. The averages of the natural logarithm of the S/N values are contoured in Figure 4b and provide a measure of filter efficiency.

The analysis shows only the responses to the filter settings for a particular type of signals and noise. It therefore inhibits generalizations for other data types. For this type of data we see that the best waveform similarities and highest S/N ratios are obtained at decreasing DOP window lengths for increasing power values. This is observed in a limited range of empirical power values and is also reported for the frequency-independent filter by Schimmel and Gallart (2003). The shorter DOP windows enable a better time resolution, but the differences between polarized and less polarized signals may decrease, which requires a larger power for improved signal discrimination. Further, we observe that for increasing power the best waveform similarities move to increasing 2σ windows. An improved frequency resolution seems to be necessary to counteract the increased sensitivity due to an increase of the power.

If one just wants to detect the signals, then the waveform distortions, in general, are not very important. The waveform distortions are caused by noise-corrupted frequency components, which will be demonstrated with the next example. Especially the smaller signal amplitudes can be unpolarized and may therefore be completely attenuated before the back-transformation to the time domain. Higher-amplitude noise affects the signals more strongly and an increased waveform

distortion is expected until all signal components are corrupted in such way that it inhibits a signal detection by a polarization approach.

Second Example: Colored-Noise Contamination

The first and the second traces in Figure 5a–c show the noise-free and noise-contaminated test data of this example. The signals 1, 2, and 3 (labeled in Fig. 5a) have different elliptical polarizations. The relative maximum amplitudes on the R and T components with respect to their Z components are depicted in the upper left of each trace in Figure 5b and c. The amplitude spectra of the three noise-free signals and the colored noise are displayed with the black lines in Figure 5d. From these curves it is visible that the low-frequency (LF) noise overlaps mostly with signal 1. The amplitude spectrum of signal 2 does nearly not interfere with the colored noise while there is partly a superposition of signal 3, especially with the high-frequency (HF) noise spectrum.

The time series at the bottom of Figure 5a–c show the filter outputs using DOP and 2σ windows of 9 and 25 samples, respectively. The power v equals 128. It is obvious from these traces that the noise has been successfully attenuated, but with alterations of the waveforms of signals 1 and 3. The signal-amplitude spectra of the normalized filter output are demonstrated with the gray lines in Figure 5d. Parts of these gray curves have higher amplitudes than the corresponding portions from the noise-free signals. This is inherent to the normalization of the filter output. Nevertheless, the comparison of the shapes of the spectra shows that the frequency components that overlap with the large-amplitude noise have been attenuated by the filter. This is expected because the degree of polarization of the signals is decreased by the noise contamination at these frequencies. It is the reason why the signal waveforms from signals 1 and 3 can not be entirely reconstructed. Signal 1 contains more noise-corrupted components than signal 3, which explains why

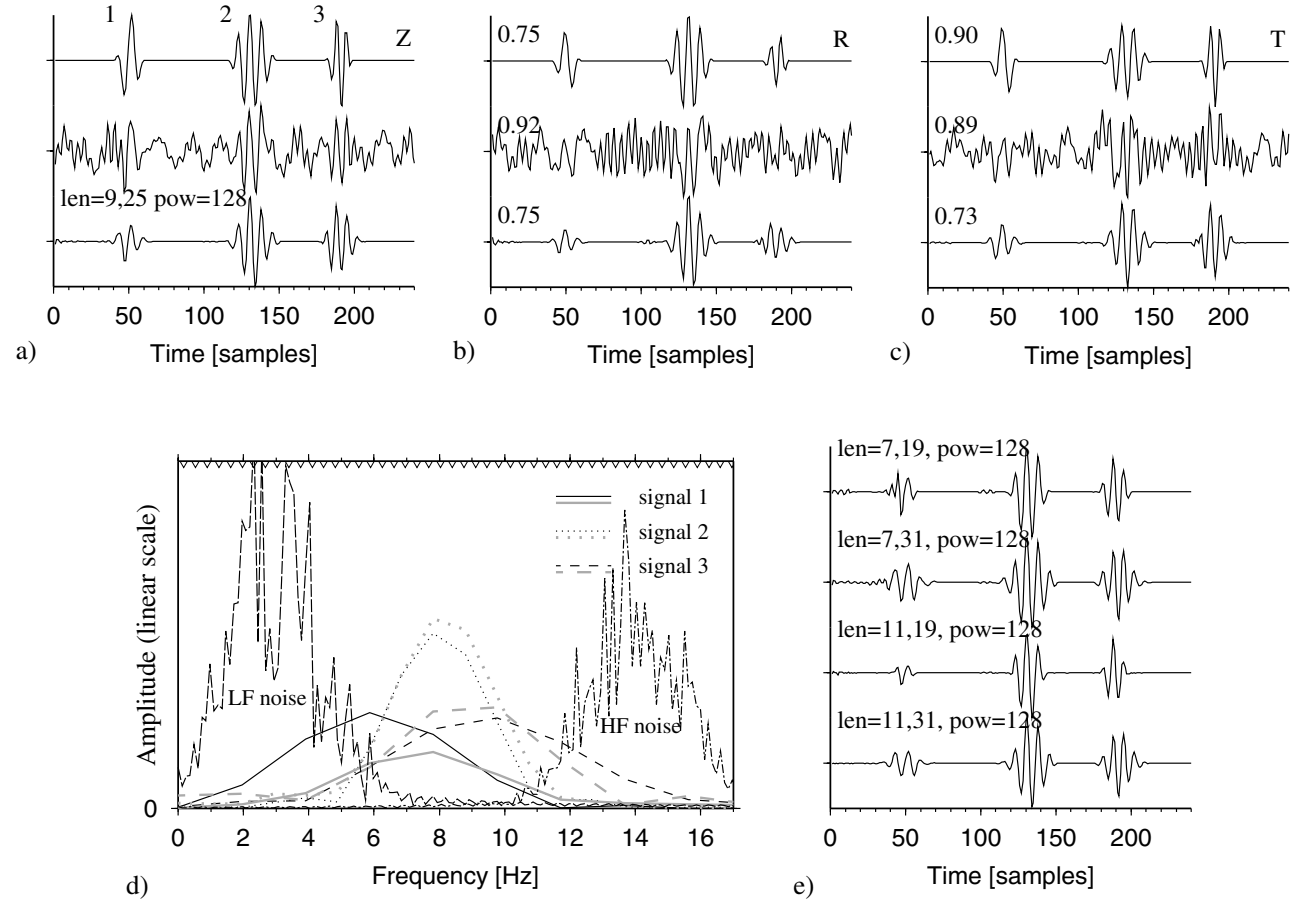

Figure 5. The traces in (a–c) are from top to bottom the noise-free data with three polarized signals, the noise-contaminated filter input, and the filtered traces. The numbers in (b) and (c) are the relative maximum amplitudes with respect to their corresponding Z components. (d) The black curves display the amplitude spectra of the three signals and of the low-frequency (LF) and high-frequency (HF) noise. The amplitude spectra of the signals on the normalized filter output are illustrated with the gray lines. The inverted triangles at the top indicate the frequencies used in the filter. (e) shows the filtered Z components for alternative filter settings. The waveforms of signals 1 and 3 are not reconstructed because of noise interferences in the frequency domain.

signal 1 is more affected by the noise. The dominant frequency components of signal 2 are not unpolarized by noise interaction, which explains the good reconstruction of signal 2. In Figure 5e we present the filtered Z components with alternative settings to access the waveform variability. It is observed that for the different filter settings signal 1 remains the signal that is less reconstructed after the filter procedure. The waveforms of signal 2 vary less and resemble most the unfiltered signal.

The example illustrates that noise and signals can be separated in the frequency domain by considering their polarization. Further, interferences between signals and noise in the frequency domain lead to decreased polarizations of the corresponding signal components and affect the signal waveform reconstructions. Large-amplitude noise can completely unpolarize the signals and may, depending on the interferences in the frequency domain, inhibit the signal detection by a polarization approach.

Third Example: Record Sections and Spatial Averaging

With densely spaced data it is recommended to include the directivity of the wave fields (slowness) and to perform a spatial averaging to increase the filter efficiency. The signal polarization is vulnerable to noise, and the spatial averaging of the degree of polarization permits removal of isolated polarized noise components or prevention of the attenuation of isolated noise-corrupted signal components.

In this example we use a theoretical record section where signals and noise share the same narrow frequency band. It is therefore a difficult task for a frequency domain filter. Figure 6a and b show the vertical and radial component record sections, respectively. The transverse components contain random noise and are not shown. The first signal is located at sample 40 and has an elliptical polarization that changes its phase by 3° per trace. The second arrival has positive slowness, is linearly polarized, and interferes with a third circular polarized signal at about sample 100. The third signal has two discontinuities at about traces 64 and 75. The fourth signal arrives at samples 160 to 170 with elliptical polarization and an amplitude that is modulated by an absolute cosine function on the Z component. The spatially coherent signals after sample 179 are amplified random noise. Entire sections have been contaminated by random noise derived from the signal-amplitude spectrum. Similar data have been used by Schimmel and Gallart (2003) with their time-domain filter.

The data have been filtered using DOP and 2σ windows of 11 and 15 samples, respectively. Every second frequency sample is used to compute the degree of polarization at 18 frequency values. In Figure 6c we show the result obtained with power $v = 16$ and using our local averaging procedure with consideration of the slowness (equation 9). Here and in the next section, we use only the median for the averages. The window includes 15 traces, three frequency samples, and three time samples. Figure 6 shows an overall noise reduction without punishing signals with spatially changing (continuous or discontinuous) polarization characteristics. Further, the coherent noise is suppressed. For Figure 6d–f the power $v = 12$ has been used. The window sizes are nine traces, three frequencies, and three time samples for Figure 6d; three traces, one frequency, and one time sample for Figure 6e; and three traces, nine frequencies, and nine time samples for Figure 6f.

The main difference between Figure 6c and d is the increased noise reduction in Figure 6c, which is mainly attributed to the larger power. Although the number of traces used in the median averaging differs by a factor of 2 no significant imprints on the signal discontinuities and zones with interfering signals are observed. Using waveforms or covariance matrices in the averaging procedure would have blurred the spatial signal discontinuities. For Figure 6e averaging is performed using only three traces. In comparison with Figure 6d a noise increase is observed. Further, we detect signals (marked by the arrow heads) that are attenuated due to unpolarization by noise. Increasing the windows for the frequency and time samples (Fig. 6f) does not prevent these attenuations but slightly decreases the overall noise amplitudes. A comparison of Figure 6e with Figure 6c and d shows that the attenuated signals marked with the arrow heads can be healed with the spatial averaging. This is because the low degree of polarization values for the isolated unpolarized signals are increased by the local averaging with slowness values that include the neighboring polarized signals. This procedure can not introduce signal energy where there is no signal energy in the input traces. For instance, the low-amplitude signal at trace 197 and sample 160 (compare Figure 6a and c) can therefore not be amplified. The amplitudes of the weights range only from 0 to 1, which inhibits introduction of new energy.

Preventing the attenuation of isolated unpolarized signals and of polarized signals with spatially changing characteristics, but suppressing isolated polarized noise, are the benefits of our local averaging procedure. These characteristics are welcomed in the processing of data where the signals interfere or where waveform changes occur, such as experienced in the transition from precritical to postcritical reflections.

Example with Real Data

Data Characteristics and Preprocessing

The abilities of our filter are further illustrated with data from a seismic refraction/wide-angle reflection profile through the Western Pyrenees to the Cantabrian Mountains in North Iberia. The source is an explosion on land, and the wave fields are recorded with almost 100 3-c stations separated by about 2.5 km. Our data correspond to shot J of a large field experiment with several profiles that were used by Pedreira *et al.* (2003) to determine the crustal structure in the Cantabrian-Pyrenean area.

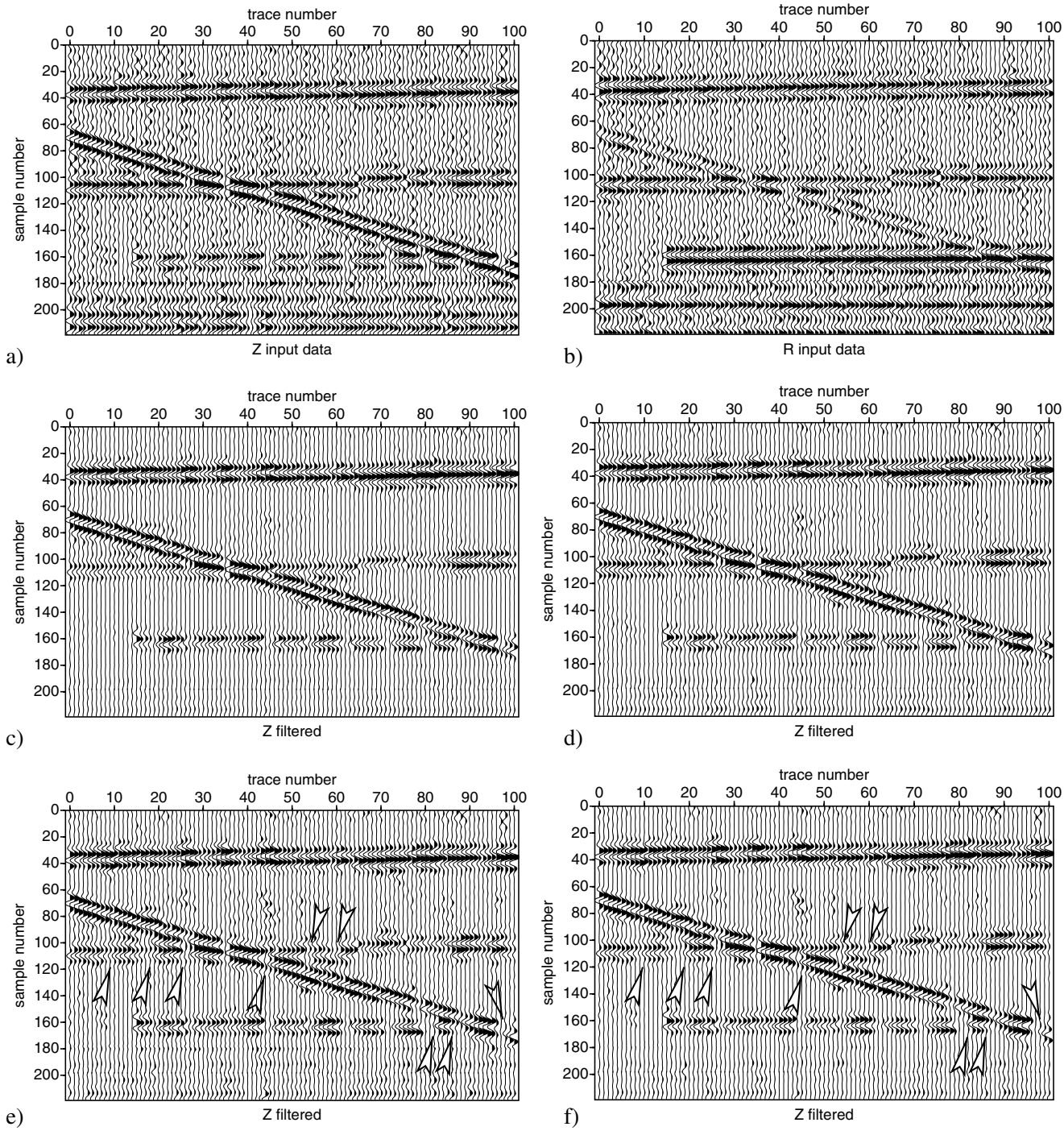

Figure 6. (a) and (b) contain the Z and R components of noisy test data. The T components contain only noise and are not shown. The first arrival (sample 40) has an elliptical polarization that changes its phase by 3° per trace. The following two signals (at trace 0: sample 70, sample 110) have linear and circular polarizations and contain abrupt arrival-time changes. The fourth signal (trace 20, sample 160) changes its ellipticity with space. Background noise is constructed from the signal-amplitude spectra. The samples larger than 180 contain spatially coherent noise. (c–f) show the filter outputs for different averaging parameters.

The preprocessing consisted in bandpassing the data using cutoff and corner frequencies of 1, 2.5, 15, and 18 Hz and resampling about one third of the traces to obtain a record section with a uniform sample interval of 10 msec. The 3-c record section is shown in Figure 7a–c. The trace amplitudes have been normalized using their root-mean-square (rms) amplitudes and the time is reduced by using a velocity of 6 km/sec to increase the visibility of the different *P* phases.

Application of Polarization Filter

Figure 8 and 9 show the filter outputs obtained with the following settings. The degree of polarization of the input data (Fig. 7) has been determined at 35 different frequencies between 1.5 and 16 Hz. The 2σ and DOP window lengths are 35 and 9 samples, respectively. The power v equals 64. Contrary to Figure 8, we average the degree of polarization in Figure 9. For the averaging we use the median in data windows of three time samples, three frequencies, and seven traces with slowness values ranging from -0.06 to 0.06 sec/km. This range excludes the direct *S* phases. The traces of the filter outputs have been balanced by their rms amplitudes.

From Figure 7 to 9 a clear energy reduction is obvious. The comparison of Figures 8 and 9 shows how the inclusion of the spatial information through our averaging procedure further cleans the data by attenuating isolated polarized features. Consequently, the coherent signals are further enhanced and the first arrivals are distinctly visible. Especially at offsets larger than 140 km, the filter with the included averaging procedure improved the visibility of the signal onsets. In the coda more or less aligned signatures are visible with the different frequency contents. The alignment strengthens that these features likely correspond to portions of the different reflection/refraction branches. Some of the aligned signals with larger amplitudes, especially on the horizontal components, can also be recognized in the filter output that is obtained without any averaging (Fig. 8).

Further, different frequency ranges are visible in the coda. A comparison with the input data shows that in some cases the higher frequencies are caused by registrations that are dominated by the higher frequencies. From the filter output alone, no conclusions can be made over the dominant frequencies in the signals. The filter output contains only the polarized frequency components of the signals. Therefore, HF features can also be a result of the attenuation of the LF components.

Although the seismic profile is from the Western Pyrenees with a very complex geology (Pedreira *et al.*, 2003), we determine the travel time curves of reflections/conversions within a simplified 1D crust model. A good signal alignment along the theoretical travel times can not be expected because of the strong lateral heterogeneities. Nevertheless, this procedure gives a rough estimate of the type of phases one may detect in the *P*-wave coda. No modeling is intended and the reader is referred to Pedreira *et al.* (2003) for a modeling study for this area. The travel time curves of the 1D velocity model are shown in Figure 10. The traces from Figure 9 are now normalized with respect to their rms amplitude between 9 sec and 12 sec and are clipped at 96% maximum amplitude. This increases the visibility of the low-amplitude coda features.

The black curves in Figure 10 indicate the portions of the wave field that are generally used in wide-angle reflection/refraction studies to infer crust structure. These are refractions through the upper crust (*Pg*) and upper mantle (*Pn*), and reflections at the top of the middle crust (*PiP*), at the top of the lower crust (*PcP*), and at the Moho discontinuity (*PmP*). The theoretical travel times for some of the *S*-wave conversions at the mentioned discontinuities are shown as gray lines without any black parts. *PiS, P30S, PcS*, and *PmS* indicate the *S*-wave conversions of the reflections at the middle crust, at a hypothetical discontinuity at 30 km, at the lower crust, and at the Moho, respectively. *Pis, P30s*, and *Pcs* mark the transmission-conversions of the *P*-wave, which impinges from below at the discontinuity. Note that the theoretical travel times of *PxS* or *Pxs* phases equal the times of *SxP* or *sxP* phases, respectively. Their amplitudes are different, and their travel times alter due to the presence of heterogeneities. In principle these phases may exist and interfere, which makes the coda more complex.

In Figure 10a–c an intermittent alignment of seismic energy to the travel time curves is observed. The first arrivals are identified as *Pg* and *Pn.* In the *Pg* coda (*Z* components) at distances longer than 60 km a *P30P* phase could explain the observed energy, which aligns intermittently until distances of 160 km. Hints of a corresponding reflection-conversion are also visible, especially on the northern components. From 60 km to about 90 km signal energy aligns at the *PiS* curve, which stands for a reflection-conversion at the middle crust. The corresponding *PiP* phase is used among others in the study of Pedreira *et al.* (2003). Further, energy seems to align intermittently at distances of about 100 km and 220 km to the theoretical *PmS* curve on the horizontal components. Other reverberations with similar slowness accompany these features. It seems strange to see a strong *PmS* at large offsets. The *PmS* signal with ray parameters, which correspond to the critical *PmP* reflection, is expected to arrive at about 75 km. At these distances a *PmS* would interfere with the direct *S* phases, which may obscure the polarization of the weaker *PmS.* The *S* phases are not enhanced because they are excluded from the considered slowness range. Besides, other aligned signals are visible in the coda.

Our brief consideration of the coda features can not replace a signal identification and interpretation study, which also is not the purpose of the present study. The data are from a complex region, which increases the ambiguities in the interpretation, and some of the aligned signals could be attributed to other phenomena. Nevertheless, it is concluded that, besides the cleaned first onsets and the overall noise reduction, one can identify coda signals that stand out

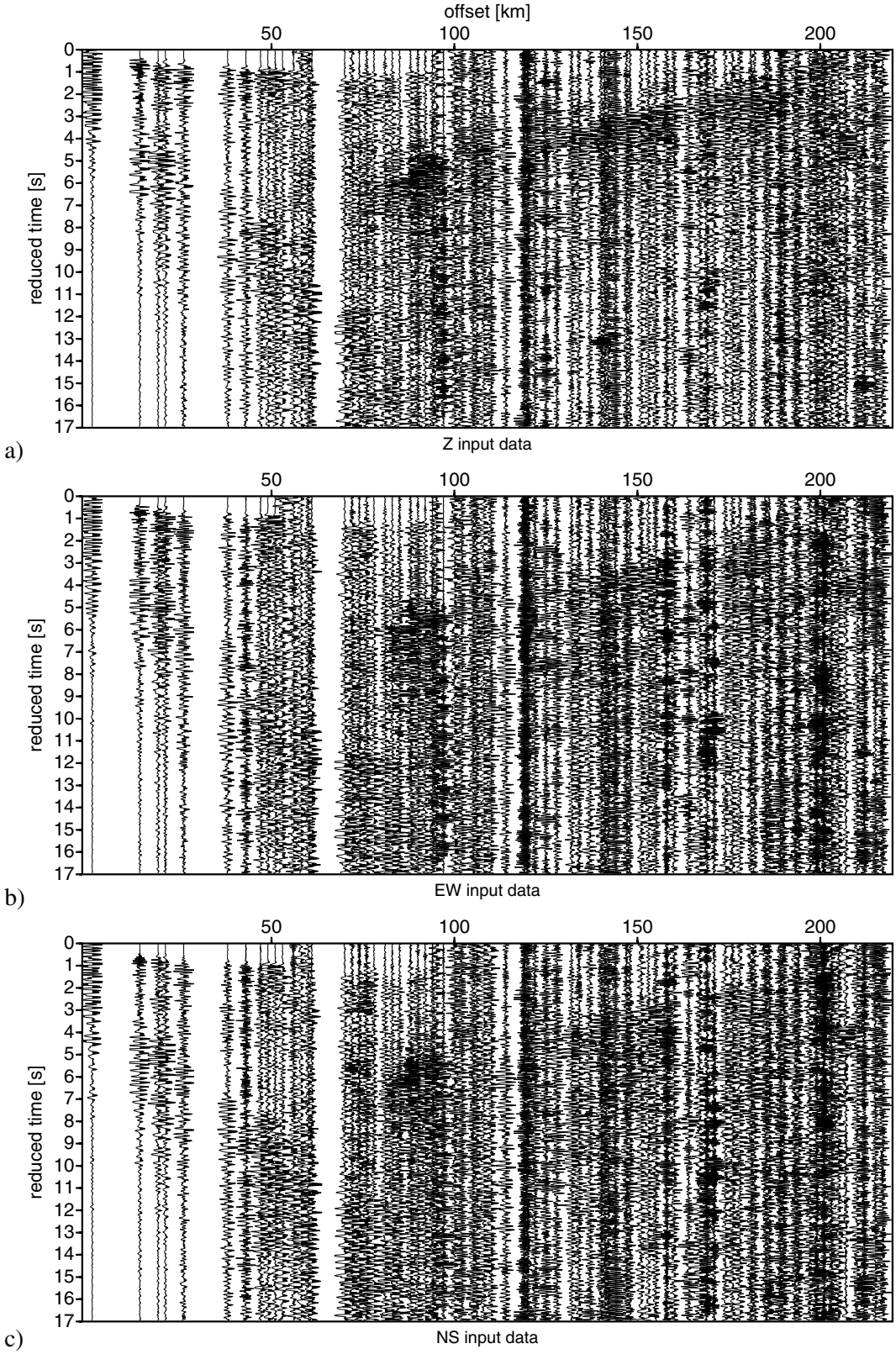

Figure 7. Refraction/wide-angle reflection data from a profile through the Western Pyrenees to the Cantabrian Mountains in North Iberia. (a), (b), and (c) contain the bandpassed vertical, eastern, and northern components. The reduction velocity is 6 km/sec. The traces are balanced by their rms amplitudes.

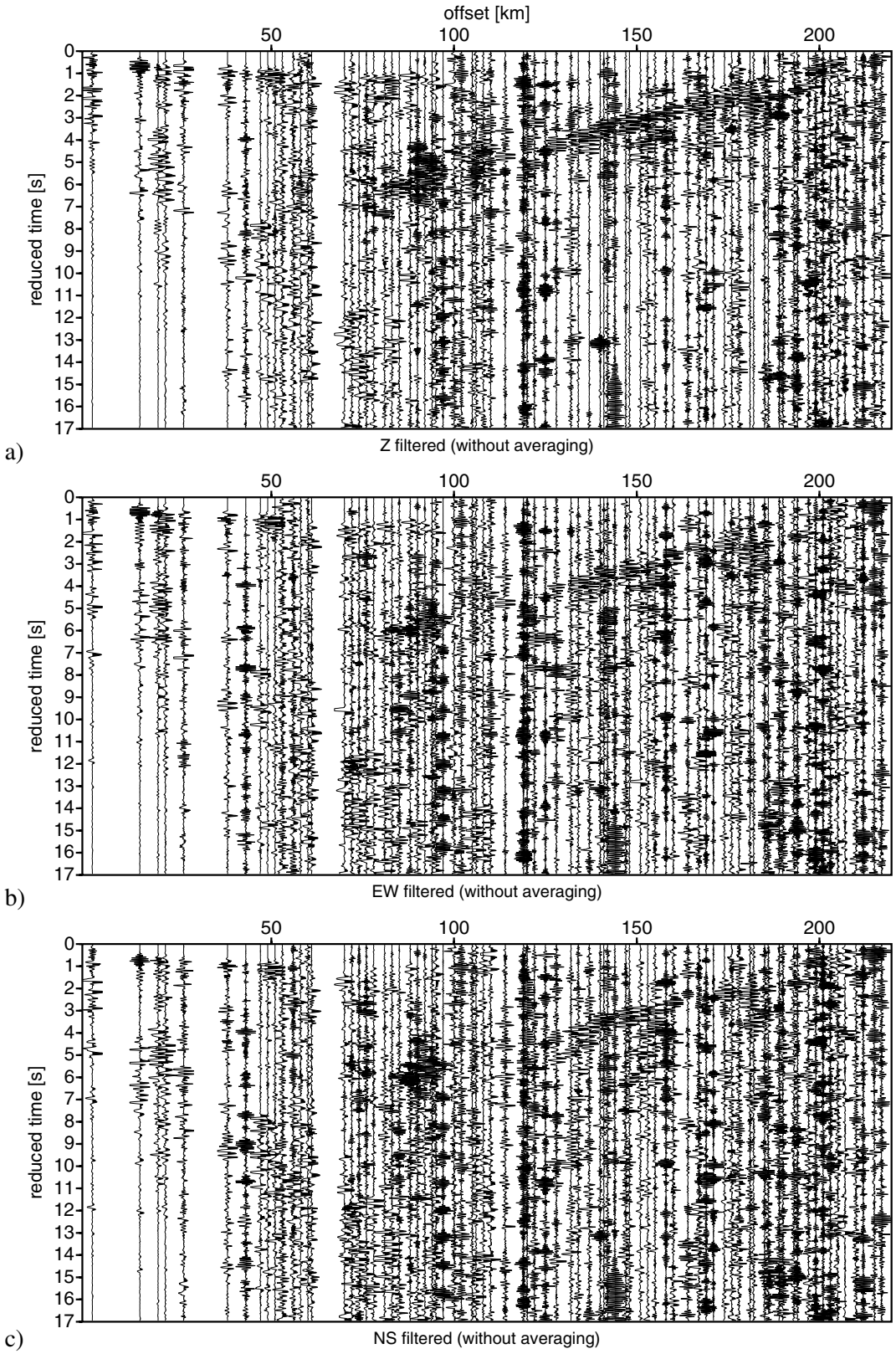

Figure 8. (a) shows the filtered vertical components of the data from Figure 7. The degree of polarization is not averaged. The traces are balanced by their rms amplitudes, and the amplitudes are clipped at 98%. (b) and (c) contain the corresponding eastern and northern components.

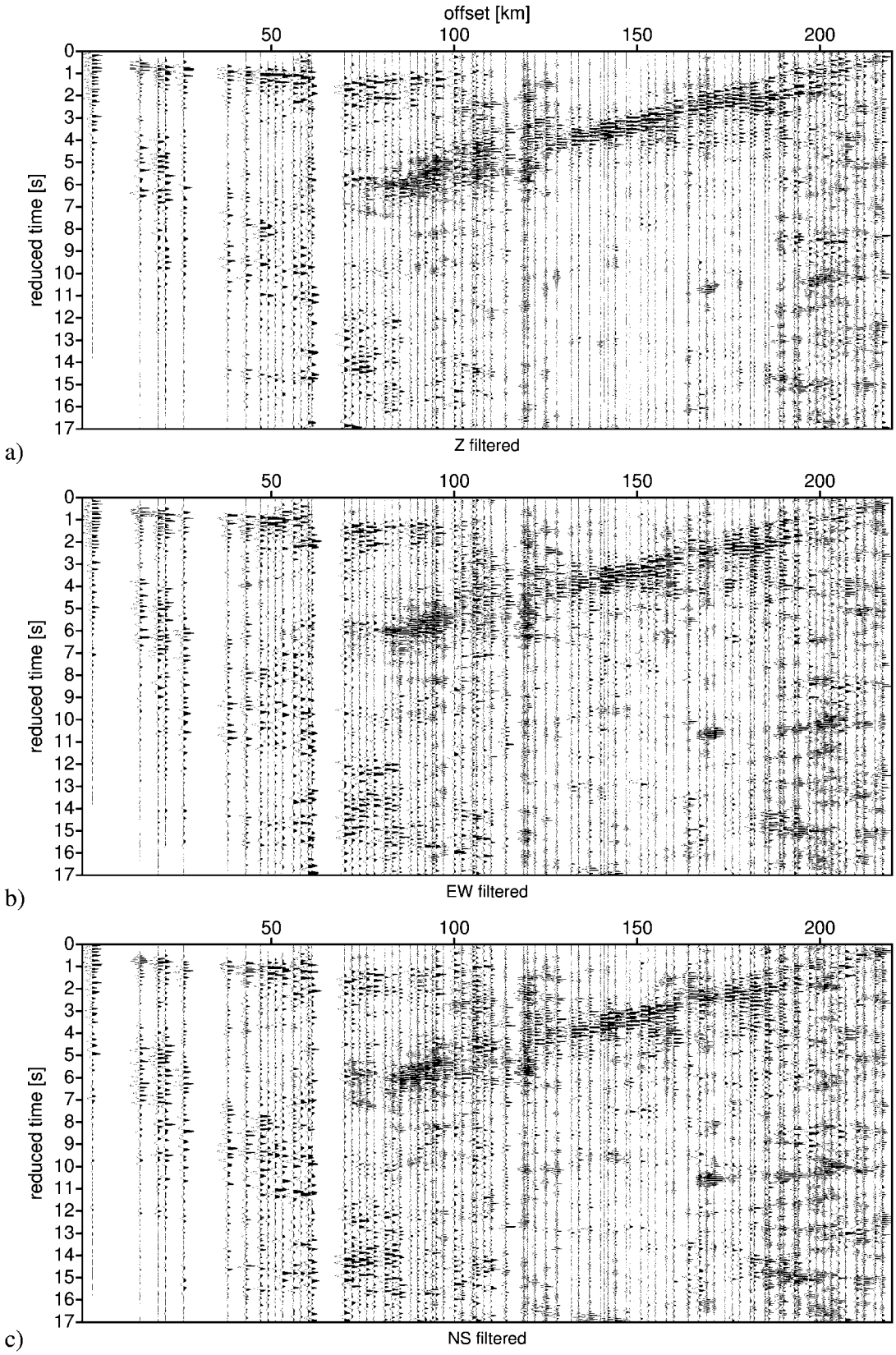

Figure 9. (a) shows the filtered vertical components of the data from Figure 7. The traces are balanced by their rms amplitudes. The amplitudes are clipped at 98%. (b) and (c) contain the corresponding eastern and northern components.

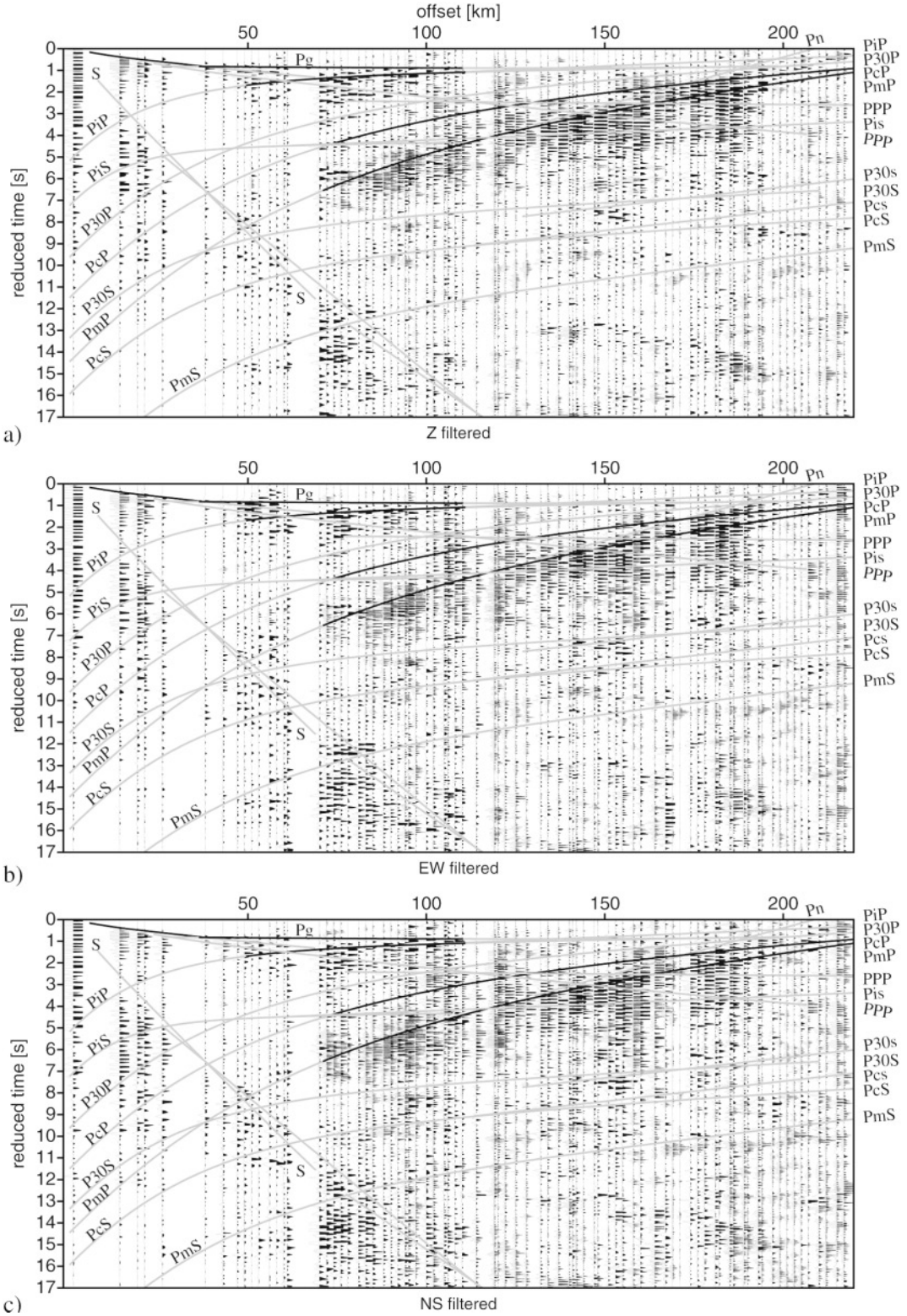

Figure 10. (a) The filtered traces from Figure 9a are balanced by their rms amplitudes between 9 and 12 sec and are clipped at 96% amplitude to increase the amplitudes in the coda. The arrival times are for a 1D crust model and can give a rough estimate of arrivals that one can expect in the coda. An interpretation is not intended. (b) and (c) are the same as (a), except for the eastern and northern components.

through their polarization, which is larger than for the noise. These signals are detected when they are aligned over several traces. Thus, depending on the data the filter can help to enhance coda signals for a refined modeling of the underlying structure. In the case of the identification of *P*-to-*S* conversions one might be able to infer the Poisson ratios.

Alternative Filter Settings

In Figure 11 the vertical component filter output is shown for alternative filter settings. We have increased the number of frequencies from 35 to 210 to obtain the section displayed in Figure 11a. This means that the polarization is now computed at all frequencies to avoid the interpolation of the degree of polarization matrix at omitted frequency values. In comparison with Figure 9a, we observe that the filter output based on all frequency components contains more energy in the coda. This is explained by the fact that the interpolation procedure acts similarly to a smoothing operator on the complete degree of polarization matrix. In other words, due to the interpolation, the degree of polarization contains fewer details and is less rough, which is reflected in an overall reduction of energy.

Figure 11b shows what happens when we increase the DOP window from 9 to 13 samples. Figure 11b shows that the first onsets are sharp and that there is less energy in the coda than in the data from Figure 9a. The increased DOP parameter implies that the degree of polarization at each frequency is based on more time samples. Through this window increase the filter now down-weights more the polarized events of short durations. This is reflected in the energy decrease of the filtered data. If one additionally increases the 2σ window then one attains the filtered traces displayed in Figure 11c. In Figure 11c we observe an increase of coda energy. For instance, at times and distances that correspond to the *S*-wave arrivals, more LF signals are observed than in Figure 11b. Further, the first onsets and their immediate coda seem to be less well resolved. This can be observed for the *Pn* phase at about 200 km and for the *Pg* phase at about 50 to 100 km. The 2σ window increase down-weights the time resolution especially of the higher-frequency signals which inherently yield a shorter time resolution than the low-frequency signals. Some short-duration signals, such as the hypothetical *P30P* signal between 60 and 100 km offset, are better resolved in Figure 11c than in Figure 11b. This is explained by the increase of the 2σ window which captures less well the time-varying properties of the polarization. It therefore counteracts a little bit the increase of the DOP window. The longer windows can yield more reliable estimates when no other signals are included in the window.

Altogether, results obtained with the different parameters can demonstrate the robust features in the data. The settings permit representation of the data in a more conservative to a more forceful fashion. The best filter settings depend much on the data at hand, the target or purpose of the data analyst, and her/his experiences and customs in viewing record sections.

Discussion

We use a new degree of polarization measure to design a data-adaptive frequency-dependent polarization filter. It is shown that the filter enhances polarized signals through the attenuation of less polarized frequency components in the local spectra. The degree of polarization that we use was originally defined by Schimmel and Gallart (2003) as a measure of the variation of an arbitrary polarization through the course of the signal. Schimmel and Gallart (2003) used this measure to construct their time-domain filter. They applied analytic signal theory and a variational approach to obtain the instantaneous polarization attributes without need of an eigen analysis. The approach presented in this study is based on a principal-component analysis to include the frequency dependence.

The filter presented here follows a simple recipe: transform the data to the time-frequency domain, weight them by their frequency-dependent degree of polarization, and perform the inverse transforms to obtain the filter output. The weight function, the degree of polarization, is the heart of the method and is not restricted to 3-c seismic data. The filter can be applied to different data types and can be tailored in many ways to account for specific data characteristics or geometries. The frequency-dependent degree of polarization down-weights the less polarized components in the frequency domain and therefore cleans the signals from noise components. Signal components that are corrupted by noise will also be attenuated before the backtransformation into the time domain. In this sense the filtered records show the polarized components of the signal waveforms rather than a complete reconstruction of the waveforms.

The main parameters of our filter are the DOP and 2σ windows and the power *v*. The DOP window length should be shorter than the signal duration but not too small to provide a representative degree of polarization. Similar to any principal component analysis, the 2σ window length should be larger than the signal duration and depends on the signal separation, dominant periods, and S/N energy ratio. Similar to other filters, playing with the different settings is required to learn the filter responses and to find a satisfying output. We recommend to start filtering with conservative settings and to interprete the robust features such as in any other study.

The spatial averaging procedure for densely spaced data is a well recognized additional tool to improve the efficiency of polarization filters. For instance, Bataille and Chiu (1991) and Jurkevics (1988) report the reduction of the estimation variance of polarization attributes when averaging the covariance data matrices of several seismic records. Depending on the nature of the data one alternatively can average the waveforms before building the covariance matrices. In our filter the averaging is applied on the degree of polarization and imprints on the data before the backtransformation into the time domain. Our local averaging considers the signal slowness and does not attenuate signals with spatially chang-

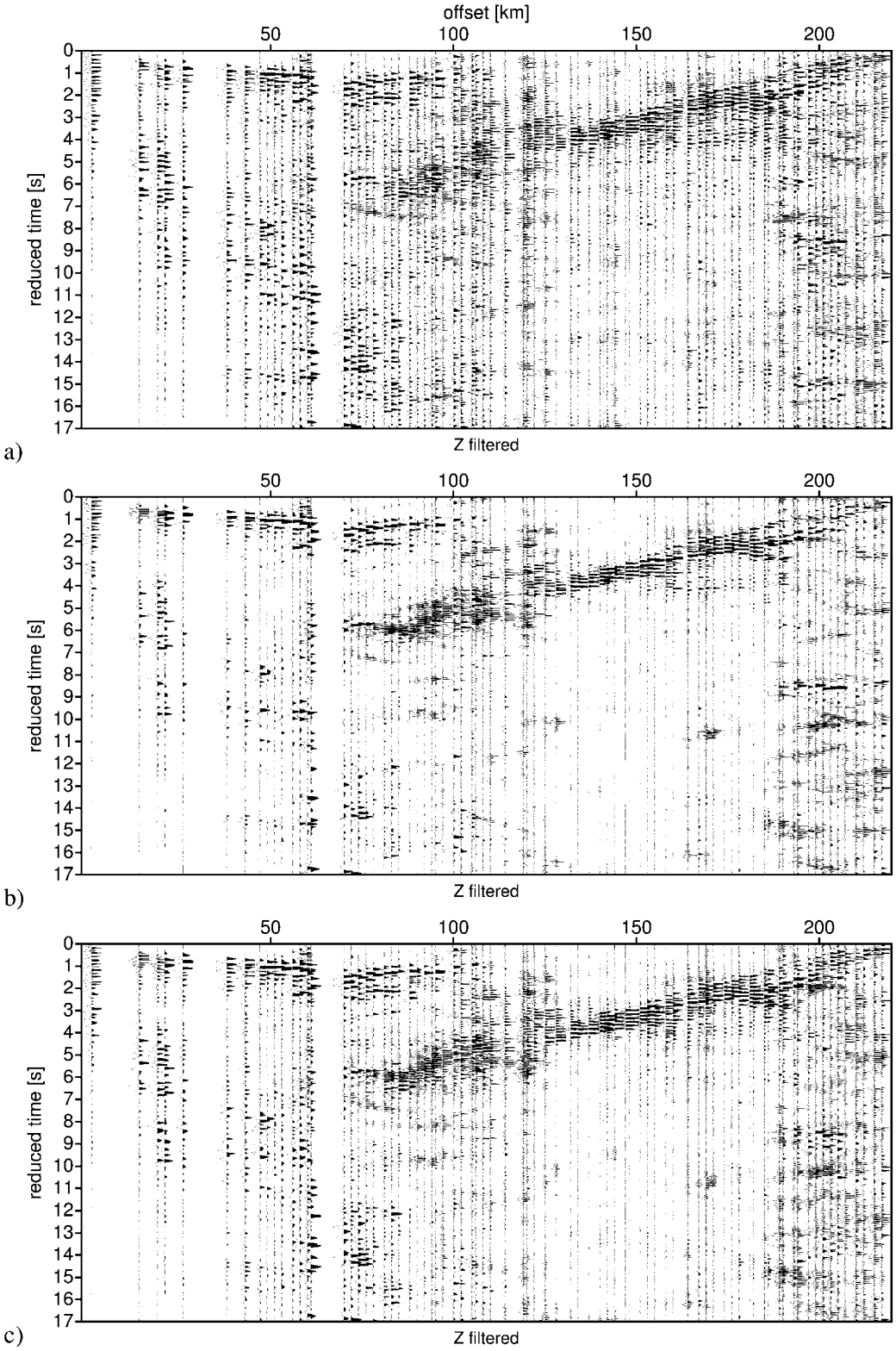

Figure 11. The vertical component filter output is shown for different filter parameters. (a) Here we have used 210 frequencies, a DOP window of nine samples, and a 2σ window of 35 samples. (b) The output is obtained with 35 frequencies, an increased DOP window of 13 samples, and a 2σ window of 35 samples. (c) The parameters are 35 frequencies, DOP window of 13 samples, and a 2σ window of 45 samples.

ing waveforms as long as the signals stay polarized. This is very important for increasing the visibility of variable signals due to heterogeneities and phase changes. Concepts that average the waveforms or the covariance matrices attenuate the variable signals and further decrease their visibility.

An alternative objective measure for the degree of polarization has been presented by Samson and Olson (1980). Their approach is based purely on the eigenvalues of the spectral matrix to determine how well the spectral matrix can be decomposed into one eigenvalue–eigenvector pair. Du *et al.* (2000) extend this method by incorporating multitaper windows to attenuate spectral leakage and by performing a noise decontamination of the data matrix. The noise estimate is obtained from a presignal data window. Altogether, these modifications translate into the degree of polarization measure.

Our filter concepts are similar and the differences are in the degree of polarization determination. Whether a local spectral component will be more or less attenuated by the different approaches depends on this real number. The degree of polarization can not alter the phase spectrum, it alters only the amplitude spectrum. Therefore, a complete signal-waveform restoration is not possible with the filters by Samson and Olson (1980), Du *et al.* (2000), and our filter, whenever the noise interferes with the signal in the frequency domain.

The degree of polarization by Samson and Olson (1980) is not designed to enhance superimposed signals with different polarization directions. These signals are decomposed into more than one eigenvalue–eigenvector pair and are therefore attenuated with their filter. This is illustrated in Figure 12. The sine and cosine wave in Figure 12a are two orthogonal polarized signals with the same frequency that appear on the *Z* and *R* components. There is no noise and no energy on the *T* component (not shown). The cosine on the *R* component has abrupt amplitude changes at samples 100, 150, and 200. Figure 12b shows the degree of polarization using our approach (first trace) and the theory of Samson and Olson (1980). The degree of polarization using the eigenvalue approach is smaller than one, as long as the composite signal can be decomposed into two principal directions. Interfering signals such as may occur at the crossovers in seismic record sections can be attenuated similarly. The composite signal is restricted to a plane in an unitary space and requires a different definition of polarization to be enhanced (Samson and Olson, 1980).

Further, it becomes obvious that the eigenvalue approach is amplitude biased since the result depends on the energy on the *R* component. This is an advantage when looking for strong arrivals but may penalize the weak signal detection, the averaging procedure for variable amplitude signals and the detection of composite signals with different polarization. Independent of the number of significant principal components (directions) our measure uses the stability of the polarization directions that correspond to the largest principal component. The measure by Samson and Olson

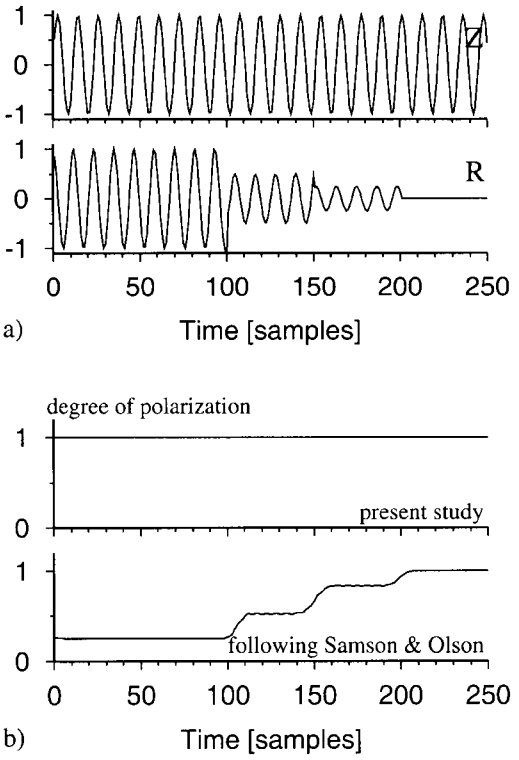

Figure 12. (a) The *Z* and *R* component consists of a sine and cosine curve with same frequency. The amplitudes on *R* change abruptly at samples 100, 150, and 200. (b) shows the degree of polarization corresponding to the test data in (a) at the frequency of the sine wave. The first trace is determined with our approach, and the second trace is determined with the theory of Samson and Olson (1980). The Samson–Olson theory measures how much of the spectral matrix is in a pure state with a purely polarized wave.

(1980) is based on a different philosophy and signal definition than our method. The differences, however, seem not to be important for the main signatures in our wide-angle test data from Figure 7. For these data we can obtain similar outputs with both filters. Both are tools for signal enhancement/detection, and it is the nature of the data and our purpose which decides which method to chose.

Conclusion

We can conclude from our examples that the filter enables frequency-dependent signal enhancement through noise suppression. This, however, is only valid for data where the signals are more polarized than the noise. The degree of polarization measure is the heart of our filter. It permits the detection and separation of time-interfering signals with different frequencies. Polarized signals that interfere in time and frequency can also be enhanced because our approach uses the largest principal direction of the decomposed composite signal. Further, the degree of polarization can be averaged for densely spaced data to increase the filter

efficiency. It is important for many applications to note that our averaging procedure does not attenuate polarized signals with varying waveforms, polarization styles, and/or amplitudes. This is meaningful in the processing of record sections with varying signals due to heterogeneities or due to phase changes in the transition from precritical to postcritical reflections. Other benefits are the suppression of isolated noise components and the prevention of the attenuation of isolated unpolarized signals. We further recall that the filter output shows the polarized components of the signal waveforms, which in the case of noise corruption must not be the complete reconstruction of the waveforms.

The filter framework itself is straightforward and permits tailoring of the measure to the different specific applications. The filter is not restricted to seismic data and more than 3-c data can be used. The polarization is subject to noise contamination, and signals with destroyed polarization on all frequency components can not be detected.

Acknowledgments

We are grateful to the researchers and technicians who contributed to the data used in this study. We also thank the Associate Editor G. Suárez and the reviewers K. Bataille and P. Earle for their constructive comments. Plots were done with Generic Mapping Tools (GMT) by Wessel and Smith (1991) and Seismic Unix by Cohen and Stockwell (1999). This research was supported by a Marie Curie Fellowship of the European Community program IHP (HPMF-CT-2001-01322).

References

Bataille, K., and J. M. Chiu (1991). Polarization analysis of high-frequency, three-component seismic data, *Bull. Seism. Soc. Am.* **81,** 622–642.

Christoffersson, A., E. S. Husebye, and S. F. Ingate (1988). Wavefield decomposition using ML-probabilities in modeling single-site 3-component records, *Geophys. J. R. Astr. Soc.* **93,** 197–213.

Cohen, J. K., and J. W. Stockwell, Jr. (1999). CWP/SU: Seismic Unix Release 33, a free package for seismic research and processing, Center for Wave Phenomena, Colorado School of Mines, Golden, Colorado.

de Franco, R., and G. Musacchio (2001). Polarization filter with singular value decomposition, *Geophysics* **66,** 932–938.

Du, Z., G. R. Foulger, and W. Mao (2000). Noise reduction for broad-band, three-component seismograms using data-adaptive polarization filters, *Geophys. J. Int.* **141,** 820–828.

Jackson, G. M., I. M. Mason, and S. A. Greenhalgh (1991). Principle component transforms of triaxial recording by singular value decomposition, *Geophysics* **56,** 528–533.

Jurkevics, A. (1988). Polarization analysis of three-component array data, *Bull. Seism. Soc. Am.* **78,** 1725–1743.

Kanasewich, E. R. (1981). *Time Sequence Analysis in Geophysics*, University of Alberta Press, Alberta, Canada.

Lilly, J. M., and J. Park (1995). Multiwavelet spectral and polarization analyses of seismic records, *Geophys. J. Int.* **122,** 1001–1021.

Montalbetti, J. F., and E. R. Kanasewich (1970). Enhancement of teleseismic body phases with a polarization filter, *Geophys. J. R. Astr. Soc.* **21,** 119–129.

Morozov, I. B., and S. B. Smithson (1996). Instantaneous polarization attributes and directional filtering, *Geophysics* **61,** 872–881.

Park, J., F. L. Vernon III, and C. R. Lindberg (1987). Frequency dependent polarization analysis of high-frequency seismograms, *J. Geophys. Res.* **92,** 12,664–12,674.

Pedreira, D., J. A. Pulgar, J. Gallart, and J. Dias (2003). Seismic evidence of Alpine crustal thickening and wedging from the Western Pyrenees to Cantabrian Mountains (North Iberia), *J. Geophys. Res.* **108,** B4, 2204, doi 10.1029/2001JB001667.

Perelberg, A. I., and S. C. Hornbostel (1994). Application of seismic polarization analysis, *Geophysics* **59,** 119–130.

Reading, A. M., W. Mao, and D. Gubbins (2001). Polarization filtering for automatic picking of seismic data and improved converted phase detection, *Geophys. J. Int.* **147,** 227–234.

Samson, J. C. (1983). The spectral matrix, eigenvalues, and principal components in the analysis of multichannel geophysical data, *Ann. Geophys.* **1,** 115–119.

Samson, J. C., and J. V. Olson (1980). Some comments on the descriptions of the polarization states of waves, *Geophys. J. R. Astr. Soc.* **61,** 115–130.

Schimmel, M. (1999). Phase cross-correlations: design, comparisons and applications, *Bull. Seism. Soc. Am.* **89,** 1366–1378.

Schimmel, M., and J. Gallart (2003). The use of instantaneous polarization attributes for seismic signal detection and image enhancement, *Geophys. J. Int.* **155,** 653–668.

Vidale, J. E. (1986). Complex polarization analysis of particle motion, *Bull. Seism. Soc. Am.* **76,** 1393–1405.

Wessel, P., and W. H. F. Smith (1991). Free software helps map and display data, *EOS, Trans. Am. Geophys. Union* **72,** 441, 445–446.

Institute of Earth Science-CSIC
c/Lluis Sole i Sabaris
s/n, 08028 Barcelona, Spain
schimmel@ija.csic.es
jgallart@ija.csic.es

Manuscript received 29 August 2003.